Front. Struct. Civ. Eng. 2023, 17(9): 1387–1399
https://doi.org/10.1007/s11709-023-0005-y

RESEARCH ARTICLE

Experimental study on the stratum applicability and mechanisms of bubble–slurry for earth pressure balance shields

Lu WANG[a,b], Wei ZHU[c*], Yongjin QIAN[a,b]

[a] *College of Civil and Transportation Engineering, Hohai University, Nanjing 210098, China*
[b] *Key Laboratory of Ministry of Education for Geomechanics and Embankment Engineering, Hohai University, Nanjing 210098, China*
[c] *College of Environment, Hohai University, Nanjing 210098, China*
[*] *Corresponding author. E-mail: zhuweiteam.hhu@gmail.com*

ABSTRACT Soil conditioning is essential for addressing the stratum applicability problem of earth pressure balance (EPB) shields. Under high water pressures, EPB shields spew water and soil when excavating coarse-grained strata. Typically, foam combined with polymers and slurry is used to solve spewing. However, in current techniques, slurry, foam, and the other agents are mixed with soil separately, their synergistic effect is seldom realized. In this study, an anionic surfactant was used to foam in bentonite slurry to form bubble–slurry to maximize the synergy between bubbles and slurry. The slump, volume stability, and permeability test of bubble–slurry-conditioned sand was conducted to examine the conditioning effect, and the stratum applicability of bubble–slurry was determined from the perspective of permeability. It was found that the conditioning effect of bubble–slurry in coarse gravel soil was excellent and could expand the applicability of EPB shields. The main stabilization mechanism of bubble–slurry is that bentonite particles provide a space barrier for bubbles. And three seepage modes of bubble–slurry-conditioned sand were innovatively defined, and the occurrence conditions of the three seepage modes were analyzed according to the permeability coefficient of sand, initial dynamic shear force of bubble–slurry, and hydraulic gradient.

KEYWORDS EPB shield, bubble–slurry, soil conditioning, stability, permeability

1 Introduction

The earth pressure balance (EPB) shield tunnel boring machine (TBM) can adapt to a variety of complex strata and urban environment, and it is the most widely used tunneling method [1–3]. Spewing generally occurs when EPB shields encounter water-rich and highly permeable coarse-grained strata [4–6]. It is necessary to inject soil conditioning agents into the pressure chamber to make the soil form a plastic-flow state [7,8]. The plastic-flow state of high-permeability coarse-grained soil features two key thresholds of fluidity and permeability. In terms of fluidity, the slump value of conditioned sand is generally required to be 150–200 mm to ensure the transmission of the screw machine [9–11]. Further, the permeability coefficient of the conditioned soil should be less than 1×10^{-3} cm/s within 90 min to balance the water pressure on the excavation surface [12].

Foam is the most common agent used in EPB shields and shows universal applicability in terms of improving the fluidity of soil [9,13–16]. However, it undergoes deformation under pressure [17,18] and may flow with water [19]. Therefore, engineers typically use foam combined with polymers or slurry in medium-coarse and coarser-grained sand [12,20,21]. Huang et al. [22] studied the fluidity and shear strength of conditioned soil, following the simultaneous addition of foam and slurry to coarse grained soil. Xu et al. [23] suggested adding slurry and polymer to cobble soil with high moisture content to improve the workability of the conditioned soil. Ling

Article history: Received Dec 6, 2022; Accepted Mar 6, 2023

et al. [24] studied the permeability of foam-bentonite slurry-conditioned sand, and found that compared with foam conditioning, bentonite slurry and foam effectively reduced the permeability of sand. However, at present, both in laboratory researches and practical engineering, the foam was pumped into the pressure chamber through the foam pipe after foaming, and the slurry was pumped into the pressure chamber through the slurry pipe. After foam contacted with soil and free water, a certain degree of defoaming occurred due to the instability of foam. However, at present, there is a lack of research on the use of bentonite slurry to protect foam, that is, there is a lack of research and application of foam and slurry to form a combined material and then add it to the soil chamber of EPB shield. As a result, the understanding of the effect of the mixture of slurry and surfactant on foaming and the synergistic effect of slurry and foam was insufficient. And most of the existing researches mainly focused on the quantitative change of the permeability of conditioned soil under different conditions [25,26], and there is little research on the seepage mode and its occurrence principle, which leads to the need for trial-and-error tests to determine the soil conditioning scheme in actual projects.

Accordingly, an anionic surfactant is used to foam in bentonite slurry to form bubble–slurry to maximize the synergy between bubbles and slurry, that is, bubbles and slurry form a combined material and then mix with soil, therefore, the bubble–slurry avoided direct contact between foam, soil particles, and pore water to significantly improved the stability of bubbles. The bubble–slurry with different bubble volume ratios (*BVR*s) were prepared and employed in slump, volume stability, and permeability tests on soils with different gradations, in order to verify its stratum applicability. And the main stabilization mechanism of bubble–slurry was analyzed. Then, three seepage modes of conditioned sand were inferred according to the change of pore water pressure during seepage process, and the initial dynamic shear force of bubble–slurry was determined through rheological tests. Finally, the occurrence conditions of the three seepage modes were discussed considering the permeability coefficient of sand, initial dynamic shear force of bubble–slurry, and hydraulic gradient.

2 Materials and methods

2.1 Materials

Six groups of soil with moisture contents of 10% were configured based on the Jinan metro line R2 and Guangzhou metro line 18, China. The particle size distributions of the soils used in the test are illustrated in Fig. 1, and the basic parameters are listed in Table 1, where d_{50}, C_u, C_c, and k are the median particle size, uniformity coefficient, curvature coefficient, and permeability coefficient of soil. The characteristic particle size d_{10} of soil was indeed widely used to evaluate the k of soil [27]. In general, when the C_u of soil was large, the k of soil was determined by fine particles, that is, the correlation between d_{10} and k was stronger. In this study, the C_u of soils was small, so there was little difference in the k of soil analyzed using d_{10} or d_{50}, and many researches adopted d_{50} to analyze k [28–30]. Therefore, d_{50} was considered as an evaluation index from the perspective of qualitative analysis in this study. Budach and Thewes [12] adjusted the application ranges of various soil conditioning agents, as indicated by Regions I–III in Fig. 1. Meanwhile, the grading curves of the three groups of soil (D, E, and F) exceed the existing grading range.

The calcium bentonite used in this study has a montmorillonite content of 60.15%. The foaming agents was synthetic surfactant (SS) with fatty alcohol

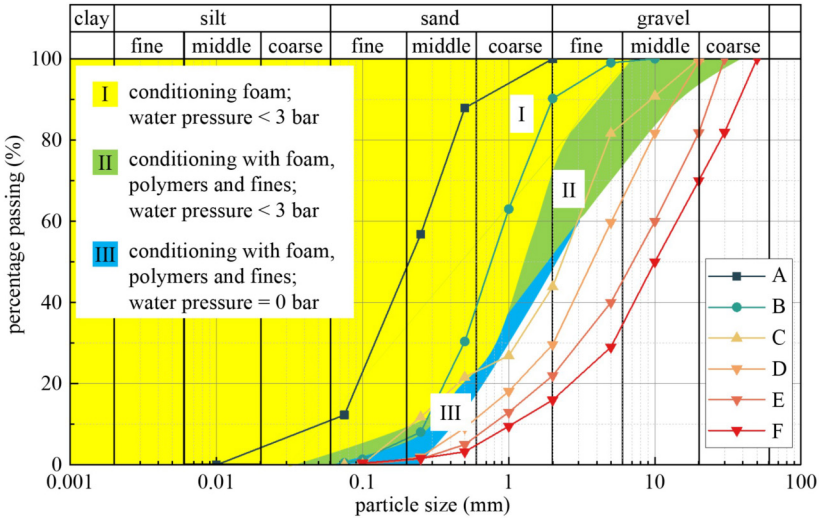

Fig. 1 Grain size distribution of the soil used in this study (1 bar = 10^5 Pa).

Table 1 Basic parameters of the soil used in the test

soil	A	B	C	D	E	F
< 0.075 mm (%)	12.3	0.5	0.08	0	0	0
d_{50} (mm)	0.21	0.76	2.32	3.74	7.15	10.06
C_u	5.40	3.48	13.50	9.26	13.30	1.17
C_c	1.07	0.99	2.02	1.53	13.42	1.73
k (cm/s)	3.94×10^{-4}	1.35×10^{-3}	4.82×10^{-3}	9.31×10^{-3}	1.52×10^{-2}	3.11×10^{-2}

polyoxyethylene ether sodium sulfate as the main raw material, which is an anionic surfactant with a density of 1.07 g/cm^3. Foam was prepared with a SS concentration (c_{ss}) of 1.0 wt%, half-life of 16 min, and foam expansion ratio of 15.5.

2.2 Methods

2.2.1 Bubble–slurry preparation

High-speed mixing (mixing speed is not less than 5000 r/min) is a common method for aqueous foam and three-phase foam generation [31–33]. First, the SS solution was added into the slurry, and then a hand-held agitator was used to stir the mixture at 5000 r/min for 3 min to make SS foam in the slurry to form bubble–slurry. The *BVR* and half-life of bubble–slurry was determined according to EFNARC [34]. The bubble–slurry volume ratio (*BSVR*), bubble–slurry injection ratio (*BSIR*), slurry concentration (c_s), and SS concentration (c_{ss}) were calculated using the following equations:

$$BVR = \frac{V_B}{V_{BS}}, \tag{1}$$

$$BSIR = \frac{V_{BS}}{V}, \tag{2}$$

$$c_s = \frac{m_b}{m_s}, \tag{3}$$

$$c_{ss} = \frac{m_{ss}}{m_L}, \tag{4}$$

where V_{BS}, V_B, and V are the volumes of the bubble–slurry, the bubbles, and excavated soil, respectively; m_b, m_s, m_{ss}, and m_L are the masses of the bentonite, slurry, SS, and mixed liquid, respectively.

2.2.2 Properties of the conditioning agents

The property test of the agents included particle size distribution, rheology, and microstructure observation. The laser particle size analyzer Malvern Mastersizer 2000 (Malvern, UK) was used to determine the median particle size (d_{50}) of slurry.

The rheology of slurry and bubble–slurry was determined by NXS-11A rotary viscometer (Chengdu Instrument Factory, China) [35]. The outer cylinder was a sample container and the inner cylinder was a rotor. The sample was placed in an outer cylinder, and the speed of the rotor was increased from 0 to 360 r/min. The outer cylinder and rotor were selected according to the viscosity of the fluid, as shown in Table 2.

Table 2 Rheological test scheme

sample ID	inner diameter of outer cylinder (cm)	outer diameter of inner cylinder (cm)	shear rate (s^{-1})
SL-1, SL-2	4	3.846	15.5–996.1
SL-3	4	3.177	3.178–204.3
SL-4, SL-5, and bubble–slurry	2	1.460	2.509–163.1

The microstructure of foam and bubble–slurry was determined by Scope. A1, Carl Zeiss Corporation optical microscope (Oberkochen, Germany). Foam or bubble–slurry was paved on the glass slide immediately after preparation, and micro images were taken with an AxioCam ICc 3 digital camera.

2.2.3 Soil conditioning

The applicability of bubble–slurry was comprehensively evaluated through slump, volume stability, and permeability tests. The slump test was referred ASTM C143 [36]. In the volume stability test, the soil sample was evenly placed in a transparent plastic cylinder with an inner diameter of 30 cm and a height of 38 cm, the initial volume and the volume after 24 h of the soil sample were recorded, then the volume change rate was obtained [34].

Constant head permeability test was used to conclude the soil permeability. The permeability coefficient of conditioned sand was measured by a self-made permeameter with a height of 65 cm and a diameter of 30 cm, and the schematic view as shown in Fig. 2. To facilitate the preparation of soil samples, the permeameter was composed of upper and lower parts. It was necessary to ensure that the contact surface was clean and dry, then placed a sealing rubber ring in the groove of the steel ring, and applied sealing grease on the contact surface, and finally connected the two parts tightly with bolts to prevent joint leakage. For the soil used in this study, this permeameter had sufficient diameter and height, and the

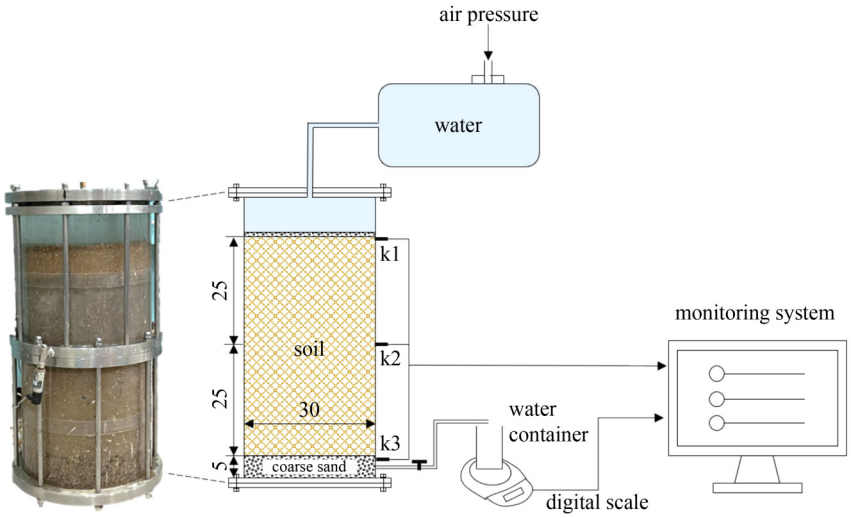

Fig. 2 Schematic view of the permeameter (unit: cm).

inner wall was smooth, thus the boundary effect was ignored. First, the sand with a particle size of 2–5 mm and a thickness of 5 cm was laid at the bottom of the permeameter as the filter layer, then poured soil sample with a height of 50 cm. Before pouring water into the permeameter, 1 cm thick coarse sand was places on the top of the soil sample to reduce the disturbance of water on the soil sample. The top cover was connected with the water tank, and the top cover of the water tank was connected with an air compressor. In the permeability test, the hydraulic gradient decreased with the decrease of water level. Therefore, the air pressure was manually increased in real time according to the reduction in water level to maintain a constant hydraulic gradient as much as possible. Three pore pressure transducers (k1, k2, and k3) were installed on the wall of the plexiglass cylinder to measure the pore water pressure. Wherein, k1 was placed in the coarse sand layer, k2 and k3 were respectively located in the middle and bottom of the soil sample, and the vertical distance between k1, k2, and k3 was 25 cm. The test process for the permeability was based on ASTM D2434-22 [37] and lasted for 90 min. The permeability coefficient of the soil was calculated using the following equation:

$$k = \frac{QL}{AHt}, \tag{5}$$

where Q is the infiltration water discharge volume at time t, L is the height of the soil sample, A is the cross-sectional area of the soil, and H is the water-level difference.

3 Results

3.1 Basic properties of soil conditioning agents

The rheology of slurry with the c_s of 10 to 30 wt% is shown in Fig. 3. The shear stress of slurry increased with the increase of c_s and shear rate. The plastic viscosity was obtained by fitting the rheological curve with Bingham model. The basic properties of the slurries are listed in Table 3. And the d_{50} of the slurry ranged from 8 to 10 μm.

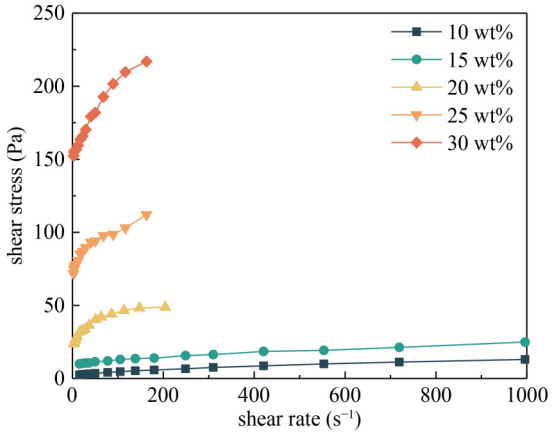

Fig. 3 Rheological curves of slurry with different concentrations.

Table 3 Basic properties of the slurry

ID	c_s (wt%)	density (g/cm^3)	plastic viscosity (Pa·s)	d_{50} (μm)
SL-1	10	1.05	0.011	8.470
SL-2	15	1.14	0.015	9.910
SL-3	20	1.17	0.131	10.070
SL-4	25	1.18	0.232	10.010
SL-5	30	1.20	0.667	10.287

Figure 4 shows the microstructure of foam and bubble–slurry with different c_s, the bubble diameter decreased with the increase of c_s, which was similar to the findings of Zhao et al. [38] and Zhong et al. [39]. Finally,

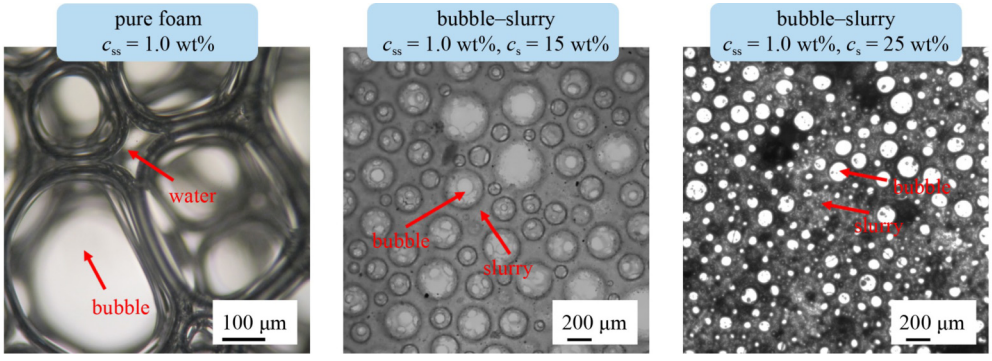

Fig. 4 Microstructures of pure foam and bubble–slurry.

four types of bubble–slurry with c_s = 25 wt% and a *BVR* of 28.57%–68.94% were selected. Their basic properties are listed in Table 4.

Table 4 Basic properties of bubble–slurry

agent ID	*BVR* (%)	half-life (h)	c_{ss} (wt%)
BS-A	28.57	216	0.4
BS-B	49.24	275	1.0
BS-C	58.51	330	1.2
BS-D	68.94	241	1.4

3.2 Slump

Figure 5 shows the effects of soil d_{50} and the *BVR* of the bubble–slurry on the slump of the conditioned soil. As indicated in Fig. 5(a), the bubble–slurry-conditioned soils exhibit desired fluidity (150–200 mm) in soils with d_{50} of 0.76–10.06 mm, while the foam-conditioned soils exhibit excessive fluidity in coarse particles. Figure 5(b) illustrates the slump increased with the *BVR*. When the *BVR* < 50%, the slump of the bubble–slurry-conditioned soil was similar to that of the slurry-conditioned soil. However, when the *BVR* exceeded 50%, the slump of the conditioned soil increased significantly.

3.3 Volume stability

Figure 6 shows the effects of the d_{50} and the *BVR* on the volume change rate of the conditioned soil within 24 h. Compared with that of the foam-conditioned soil (12%–28%), the rate of change of the bubble–slurry-conditioned soil volume was between 2% and 12%, which represents a relatively stable state. This trend reveals that the bubble–slurry has a more stable volume in coarser-grained soils. There is an inflection point in the volume change rate curve of foam-conditioned soil, because when the *w* was 10% and d_{50} < 2.32 mm, part of the bubbles broke due to lack of free water in the pores when mixing with the soil. An increase in the *BVR* leads to a linear decrease in stability, as shown in Fig. 6(b). The rate of change of the volume of the bubble–slurry-

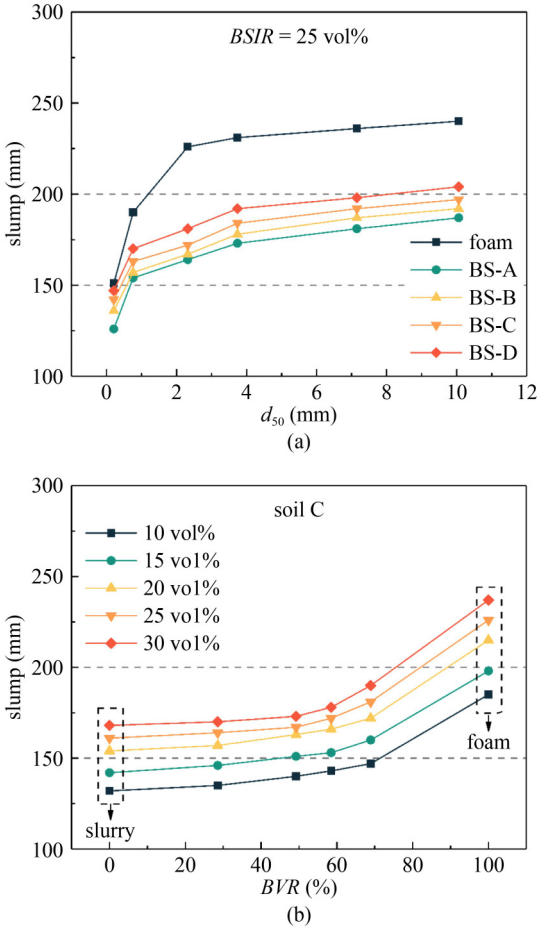

Fig. 5 Median particle size of sand and *BVR* values versus slump values: (a) median particle size of sand; (b) *BVR*.

conditioned soils with the largest *BVR* (68.94%) was approximately equal to 1/3 of the value for the foam-conditioned soil.

3.4 Permeability coefficient

3.4.1 Effect of d_{50} of soil on permeability coefficient

The *k* of conditioned soil increases with the increase of d_{50} of sand. After adding 25 vol% bubble–slurry for

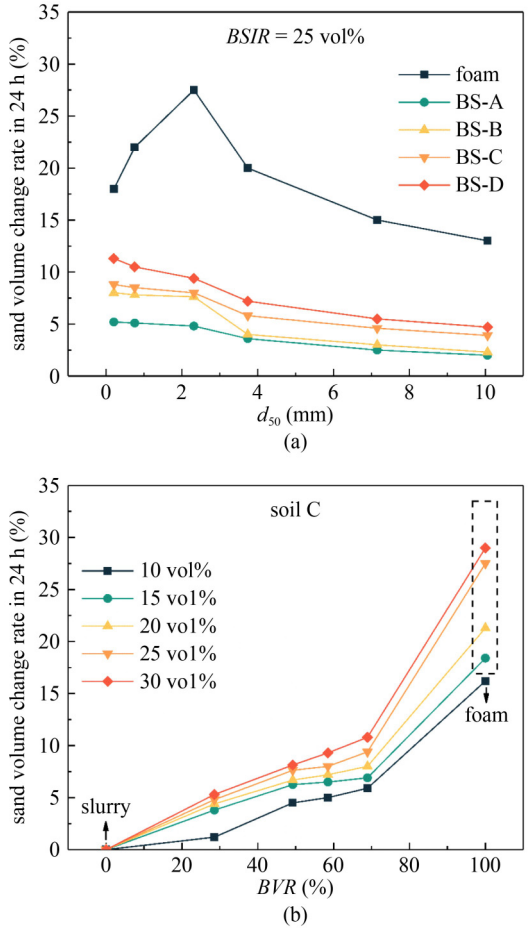

Fig. 6 Median particle size of sand and *BVR* values versus sand volume stability: (a) median particle size of sand; (b) *BVR*.

conditioning, k can be reduced by more than one order of magnitude when hydraulic gradient i was 4, and most of the k are lower than 1×10^{-3} cm/s (Fig. 7). However, bubble–slurry BS-C and BS-D could not meet the permeability requirements of soils with $d_{50} > 7.15$ mm.

3.4.2 Effect of the *BVR* on permeability coefficient

As illustrated in Fig. 8, in the case of soil C (d_{50} = 2.30 mm), the conditioning effect of the bubble–slurry on k was similar to that of the slurry (*BVR* = 0) when the *BVR* < 50%. However, when the *BVR* increased from 50% to 70%, the k of conditioned soil increased significantly. As illustrated in Fig. 9, we also demonstrated that the effect of bubble–slurry conditioning was better than that of traditional slurry and foam directly mixed with soil (referred to as foam−slurry-conditioned sand). The reason for this is that the bubbles of bubble–slurry are encapsulated by the slurry and do not directly come in contact with the soil particles and pore water; this protects the overall structure of the bubble–slurry.

3.4.3 Effect of hydraulic gradient on permeability coefficient

Figure 10(a) illustrates that, for soil C, k of the foam-conditioned soil increased significantly with increasing i. And when i was below 10, the k of the four types of bubble–slurry-conditioned soils changed marginally. However, for soil F, the k of almost all the conditioned soils increased with increasing i (Fig. 10(b)), except for the k of conditioned soils by slurry, BS-A, and BS-B, which remained relatively stable below an i of 4. And when the i was greater than 10, the k of the slurry-conditioned soil significantly increased.

3.4.4 Pore water pressure of conditioned sand

For determining the seepage mode of the conditioned sand, when the amount of agent was 25 vol%, the water pressure P_w was 50 kPa, and the i was 10, the pore water pressure of foam-conditioned soil, slurry-conditioned sand and bubble–slurry-conditioned sand in the 90 min

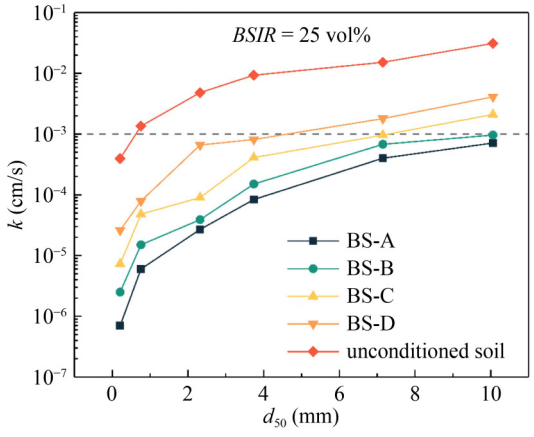

Fig. 7 Effect of median particle size of sand on permeability coefficient of conditioned sand (P_w = 20 kPa, i = 4).

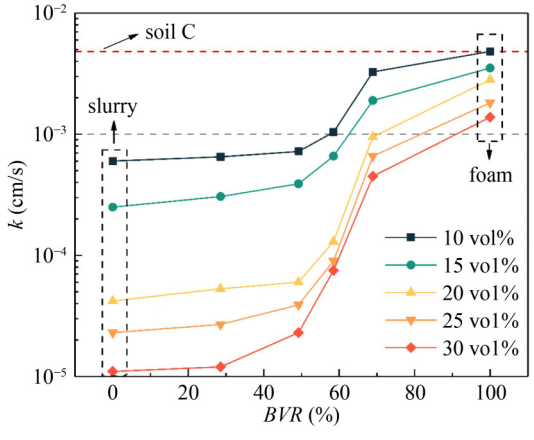

Fig. 8 Effect of *BVR* on permeability coefficient of conditioned sand (P_w = 20 kPa, i = 4).

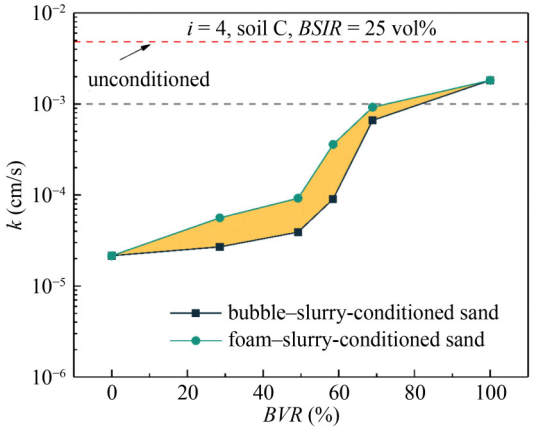

Fig. 9 Difference of permeability coefficient between bubble–slurry-conditioned sand and foam−slurry-conditioned sand.

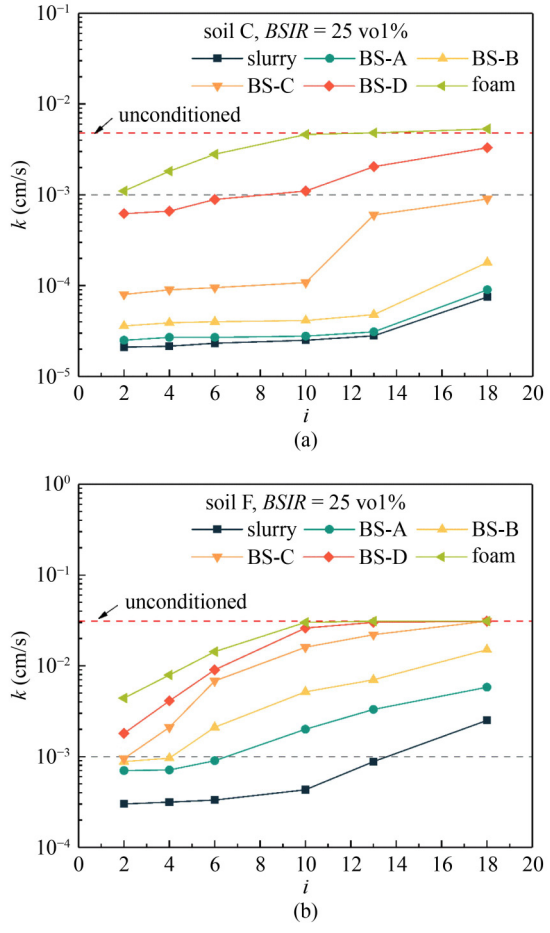

Fig. 10 Effect of hydraulic gradient on permeability coefficient of conditioned sand: (a) soil c; (b) soil F.

permeability test are explored below. The pore water pressure at k2 and k3 positions of foam-conditioned sand decreased rapidly at the initial stage of seepage (Fig. 11(a)), indicating that the foam blocked the pores and reduced the seepage channel of sand. However, the stage of foam plugging the pores was short (30 s). Then there was an increase in pore water pressure as foam was forced out of the soil. If the drain valve was closed at this time, the pore pressure at the bottom of the conditioned sand would exceed the pore pressure at the top under the hydrostatic state. It is indicated that connected seepage channels had been formed. The pore water pressure of

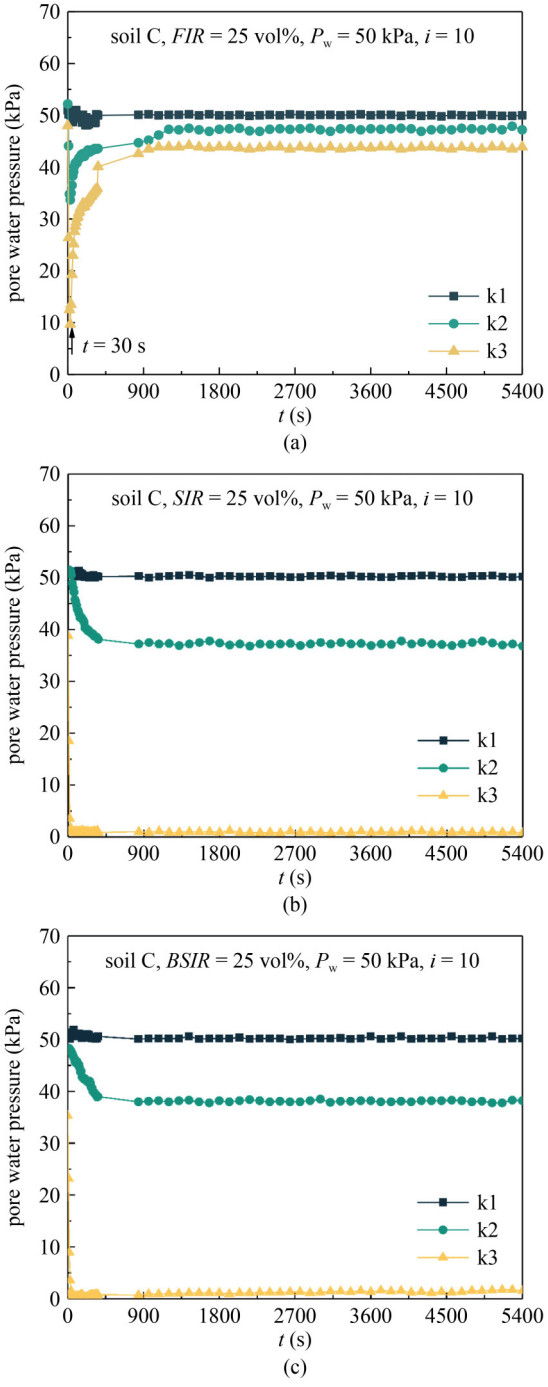

Fig. 11 Pore water pressure of conditioned sand: (a) foam-conditioned sand (FIR: foam injection ratio); (b) slurry-conditioned sand (SIR: slurry injection ratio); (c) bubble–slurry-conditioned sand.

slurry-conditioned sand is shown in Fig. 11(b). With the increase of time, the pore water pressure of k2 and k3 gradually stabilized, which were 37.2 and 0.9 kPa respectively. The permeability characteristic of bubble–slurry-conditioned sand was between that of slurry-conditioned sand and that of foam-conditioned sand (Fig. 11(c)), the pore water pressure of k2 and k3 of conditioned sand with BS-B stabilized at 38.1 and 1.3 kPa, respectively. It means that the slurry and bubble–slurry could steadily plug some pores.

4 Discussion

4.1 Stratum applicability of the bubble–slurry

Based on the above test results, the stratum applicability range of the bubble–slurry is summarized in Fig. 12 from the perspective of conditioned sand permeability. The medium-coarse and coarse sand located in Region II can be conditioned with bubble–slurry provided i does not exceed 18. As reported previously, the maximum i reached 10.2 [19]. Accordingly, it can be inferred that the bubble–slurry agent can be used extensively in Region II. Moreover, the gravelly soil located in Region III can be conditioned with bubble–slurry when $i < 6$. The three curves (a), (b), and (c) in Fig. 12 represent the boundaries of the previously reported application ranges for soil conditioning agents [12]. A comparison of these three curves with the application range of bubble–slurry determined in this study reveals that the application of bubble–slurry can expand the applicability of EPB shields in coarse-grained soil. The stratum applicability of conditioned soil also needs to consider the compressibility [40] and shear strength [41]. Therefore, the compressibility and shear strength of bubble–slurry-conditioned sand will be further studied to improve the view.

4.2 Stabilization mechanism of bubble–slurry

Schematic diagram of structure of bubble–slurry is shown in Fig. 13. Bentonite particles would hydrate in water to form the bound water [42]. The hydrophilic groups of the anionic surfactant combined with the bound water of the bentonite, the desorption energy of bentonite particles on the liquid film was greater than that of surfactant molecules, which increased the viscosity of the liquid film and inhibited the drainage of liquid film [24,38]. Suitable solid particles could form a space barrier between bubbles [43–46], the bentonite particles between bubbles restricted the gas transmission, hindered the coalescence of bubbles, and improved bubbles stability.

The cationic-anionic surfactant mixtures are commercial surfactants commonly used in EPB shields construction sites. Cationic surfactants in the mixtures are mostly used as foam stabilizers, and anionic surfactants are the main materials for foaming. In this study, an anionic surfactant was used to foam in the slurry, and the slurry played a bubbles-stabilizing effect, and even if cationic surfactants were not used as foam stabilizers, the stability of bubble–slurry was significantly higher than that of pure foam. Therefore, these experiments in this study could provide suggestions for the soil conditioning when the EPB shields tunnelling in coarse soil. Meanwhile, the difference of foaming and bubbles stability of anionic, cationic, and anionic-cationic mixed surfactants in bentonite slurry is worth further study. The interaction between surfactant and particles involves zeta potential, particle hydrophobicity, surface tension and other surface-interface characteristics [47–50], and we are researching the details.

4.3 Three seepage modes and occurrence conditions of bubble–slurry-conditioned sand

On account of the difference of sand gradation and

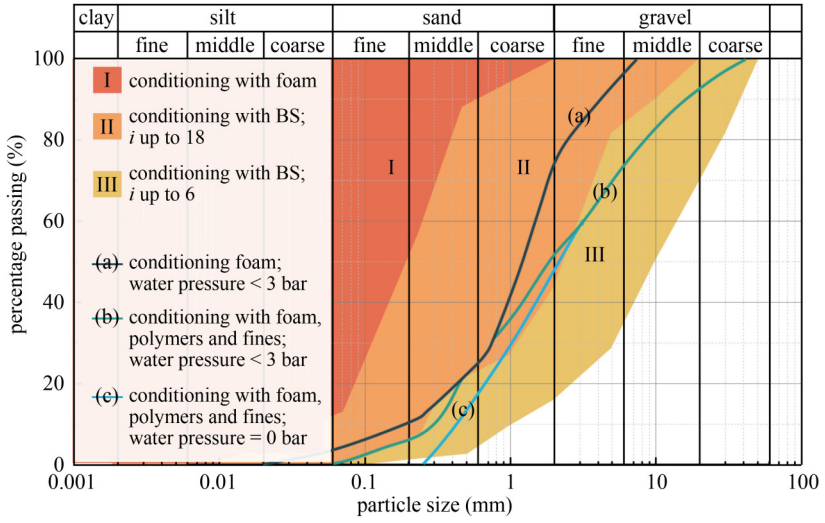

Fig. 12 Stratum applicability range of the bubble–slurry.

hydraulic gradient, the bubble–slurry-conditioned sands show three seepage modes, as shown in Fig. 14, the horizontal arrow with solid line and the horizontal arrow with dashed line indicated the initial pore water pressure and change trend of pore water pressure during permeability, respectively. When the sand pores and hydraulic gradient are small, bubble–slurry plugs the pores, and the pore water pressure would gradually decrease along the depth of the conditioned sand, and only pore water would pass through the seepage channels (Fig. 14(a)). When the sand pores are small and the hydraulic gradient increases, the fine particles of the bubble–slurry may pass through the seepage channels with water, and the pore water pressure in the conditioned sand gradually increases with time (Fig. 14(b)). When the sand pores and hydraulic gradient get even larger, the bubble–slurry would flow out smoothly, and the pore water pressure would rapidly increase (Fig. 14(c)).

The permeability mode of bubble–slurry is determined by the Jamin effect of bubbles and the blockage effect of bentonite particles [39]. However, it is difficult to discuss these two effects independently in bubble–slurry system. To explore the occurrence conditions of different permeability modes of bubble–slurry-conditioned sand, the rheological properties of bubble–slurry and pure slurry were analyzed, as shown in Fig. 15. Bubble–slurry is a non-Newtonian fluid, the existence of initial dynamic shear force τ_0 is evident, and the Herschel−Bulkley model fit the experimental data more accurately. Notably, the τ_0 gradually decreased as the *BVR* increased. It means that the bubble–slurry in the pores only begins to flow when hydraulic gradient i is greater than initial hydraulic gradient i_0 [35]. It is conducive to plugging the formation [51], and this is the main reason for the difference in response of different bubble–slurry-conditioned soils to i. It should be noted that in practical engineering, the i between the excavation face and the outlet of the screw conveyor was usually 2–5, and the maximum i was 10.2 [19]. Meanwhile, the i between the support pressure provided by the pressure chamber and the groundwater pressure on the excavation surface was smaller. Therefore, the support pressure provided by the pressure chamber had less effect on the k of the conditioned soil at the excavation surface.

The seepage mode of bubble–slurry-conditioned sand is closely related to hydraulic gradient, initial dynamic shear

Fig. 13 Schematic diagram of structure of bubble–slurry.

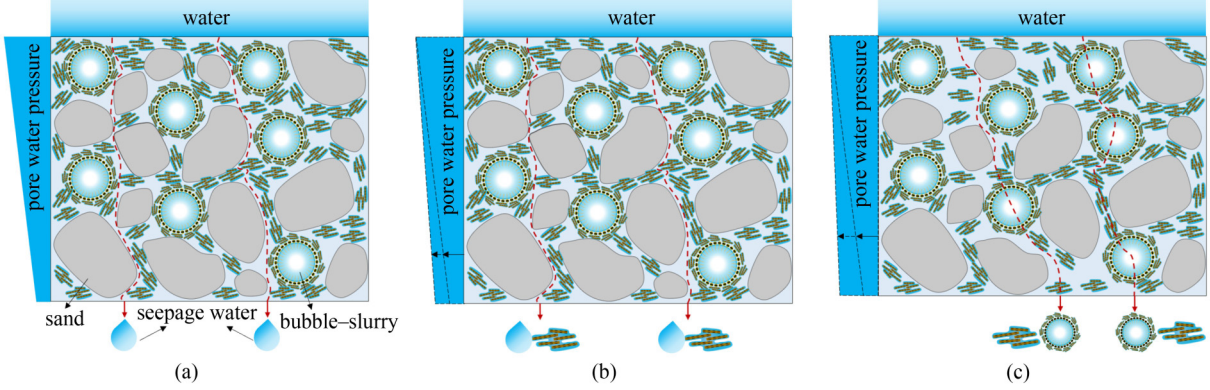

Fig. 14 Seepage modes of bubble–slurry-conditioned sand: (a) mode A; (b) mode B; (c) mode C.

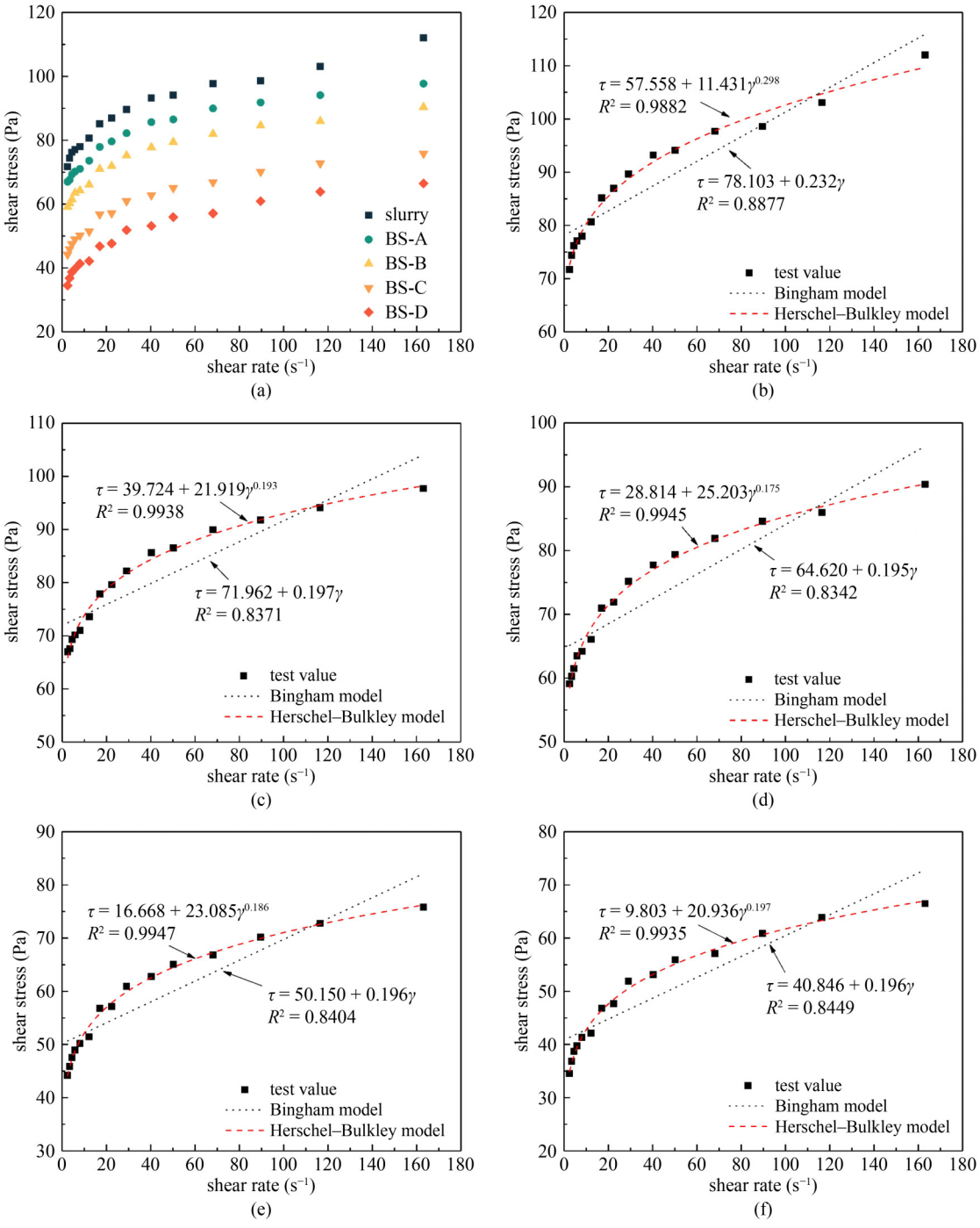

Fig. 15 Rheological properties: (a) rheological curves of slurry and bubble–slurry; rheological parameter fitting curve of (b) slurry; (c) BS-A; (d) BS-B; (e) BS-C; (f) BS-D.

force of bubble–slurry, gradation and pores diameter of sand. The gradation and pores diameter determine the permeability coefficient of sand. Therefore, the occurrence conditions of three seepage modes were analyzed based on the initial dynamic shear force of bubble–slurry, hydraulic gradient and permeability coefficient of sand, as shown in Fig. 16. Figure 10 shows the permeability coefficients of soil C and F conditioned by bubble–slurry under different hydraulic gradients, therefore, the permeability coefficient threshold in Fig. 16 was determined based on the permeability coefficients of unconditioned soil C and F. When the permeability coefficient of the formation did not exceed 4.82 × 10^{-3} cm/s, and the hydraulic gradient was above the dashed line *a* or below the solid line *b*, the permeability characteristics of bubble–slurry-conditioned sand were modes C and A, respectively. Similarly, when the permeability coefficient of the formation was between

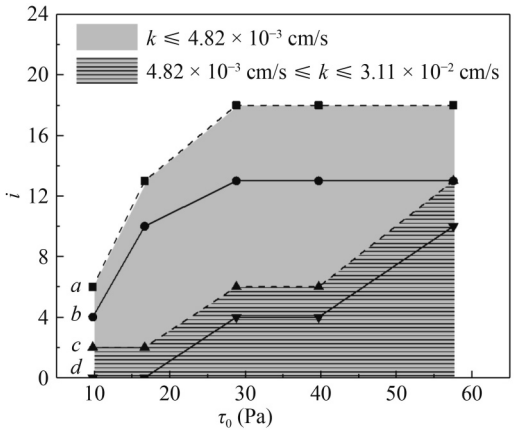

Fig. 16 Hydraulic gradient versus initial dynamic shear force of bubble–slurry.

4.82×10^{-3} and 3.11×10^{-2} cm/s, and the hydraulic gradient was above the dashed line *c* or below the solid line *d*, the permeability characteristics of bubble–slurry-conditioned sand were modes C and A, respectively. When the hydraulic gradient was equal to the initial hydraulic gradient of bubble–slurry, the permeability of bubble–slurry-conditioned sand was mode B. Furthermore, when EPB shield is slowly excavated or stopped, it is safest to make the permeability of the conditioned sand as mode A. However, when the excavation speed of EPB shield is fast, the mode B should be considered to reduce the cost, but it needs to be determined by permeability tests that the bubble–slurry-conditioned sand would maintain low permeability before being discharged from the screw conveyor.

This study compared the conditioning effect of foam and bubble–slurry on the scale of laboratory test, and bubble–slurry exhibited better performance. The laboratory tests can reflect the effect of field application to a certain extent, so it can be reasonably believed that the research results in this study can contribute to practical projects in a certain extent. During the stirring of the pressure chamber and the discharge of the screw conveyor, the interaction between the bubbles and the slurry may be disturbed, it is necessary to further study the application of bubble–slurry in practical engineering.

5 Conclusions

This paper proposed bubble–slurry based on surfactant foaming in slurry to maximize the synergy between bubbles and slurry. Various bubble–slurry and soil conditions were investigated to verify its stratum applicability. Finally, three seepage modes and occurrence conditions of bubble–slurry-conditioned sand were defined. The following conclusions can be drawn.

(1) Bubble–slurry achieves a better conditioning effect than foam and the simultaneous use of foam and slurry. The effects of bubble–slurry pertain to the fact that prior mixing causes the slurry and bubbles to form a combined material. According to the test results of conditioned sand fluidity, volume stability and permeability, bubble–slurry can be fully applied to medium-coarse and coarse sandy soil, as well as to gravel soil, when *BVR* and hydraulic gradient do not exceed 28.57% and 6, respectively. The compressibility and shear strength of bubble–slurry-conditioned sand will be further studied.

(2) The main stabilization mechanism of bubble–slurry is that bentonite particles provide a space barrier for bubbles, restrict the gas transmission between bubbles, enhance the strength and inhibit the drainage of liquid film, the stability of bubbles is improved. The interface characteristics of bubble–slurry is being further studied.

(3) Three seepage modes for bubble–slurry-conditioned sand is proposed. The seepage mode is mainly determined by sand permeability coefficient, hydraulic gradient, and initial dynamic shear force of bubble–slurry. With the increase of sand permeability coefficient and hydraulic gradient, the initial dynamic shear force of bubble–slurry is required to be higher. In engineering application, the excavation speed of EPB shield should also be considered, therefore, the bubble–slurry-conditioned sand could be switched between modes A and B to reduce costs.

Acknowledgements This study was funded by National Key R&D Program of China (2022YFC3202705), the Fundamental Research Funds for the Central Universities (B200203081), and the Postgraduate Research and Practice Innovation Program of Jiangsu Province (KYCX20_0436).

Conflict of Interest The authors declare that they have no conflict of interest.

References

1. Lei H Y, Zhang Y J, Hu Y, Liu Y N. Model test and discrete element method simulation of shield tunneling face stability in transparent clay. Frontiers of Structural and Civil Engineering, 2021, 15(1): 147−166
2. Liao S M, Liu J H, Wang R L, Li Z M. Shield tunneling and environment protection in Shanghai soft ground. Tunnelling and Underground Space Technology, 2009, 24(4): 454−465
3. Martinelli D, Peila D, Campa E. Feasibility study of tar sands conditioning for earth pressure balance tunnelling. Journal of Rock Mechanics and Geotechnical Engineering, 2015, 7(6): 684−690
4. Liu P F, Wang S Y, Ge L, Thewes M, Yang J S, Xia Y M. Changes of Atterberg limits and electrochemical behaviors of clays with dispersants as conditioning agents for EPB shield tunnelling. Tunnelling and Underground Space Technology, 2018, 73: 244−251
5. Wang L, Zhu W, Qian Y J, Xu C, Hu J N, Xing H T. Phenomenon and critical conditions of chamber soil sliming during EPB shield tunneling in water-rich weathered diorite: Case study of Jinan

Metro, China. Advances in Civil Engineering, 2020, 2020: 1−15
6. Zheng G, Dai X, Diao Y. Parameter analysis of water flow during EPBS tunnelling and an evaluation method of spewing failure based on a simplified model. Engineering Failure Analysis, 2015, 58: 96−112
7. Merritt A S, Mair R J. Mechanics of tunnelling machine screw conveyors: Model tests. Geotechnique, 2006, 56(9): 605−615
8. Peila D. Soil conditioning for EPB shield tunnelling. KSCE Journal of Civil Engineering, 2014, 18(3): 831−836
9. Baghali H, Chakeri H, Sharghi M, Dias D. Effect of soil moisture and granulometry on soil conditioning for EPB-TBM tunneling: Case study. Journal of Testing and Evaluation, 2021, 49(1): 355−371
10. Peila D, Oggeri C, Borio L. Using the slump test to assess the behavior of conditioned soil for EPB tunneling. Environmental & Engineering Geoscience, 2009, 15(3): 167−174
11. Vinai R, Oggeri C, Peila D. Soil conditioning of sand for EPB applications: A laboratory research. Tunnelling and Underground Space Technology, 2008, 23(3): 308−317
12. Budach C, Thewes M. Application ranges of EPB shields in coarse ground based on laboratory research. Tunnelling and Underground Space Technology, 2015, 50: 296−304
13. Galli M, Thewes M. Rheological characterisation of foam-conditioned sands in EPB tunneling. International Journal of Civil Engineering, 2019, 17(1): 145−160
14. Langmaack L, Lee K F. Difficult ground conditions? Use the right chemicals! Chances-limits-requirements. Tunnelling and Underground Space Technology, 2016, 57: 112−121
15. Quebaud S, Sibai M, Henry J P. Use of chemical foam for improvements in drilling by earth-pressure balanced shields in granular soils. Tunnelling and Underground Space Technology, 1998, 13(2): 173−180
16. Tao L M, Chen Z T, Cui J, Wang H W, Fang Y. Experimental methods to assess the effectiveness of soil conditioning with foam in fully weathered granite. Advances in Materials Science and Engineering, 2019, 2019: 1−12
17. Wan Z E, Li S C, Yuan C, Zhao S S, Wang M L, Lu Q L, Hou W. Soil conditioning for EPB shield tunneling in silty clay and weathered mudstone. International Journal of Geomechanics, 2021, 21(9): 06021020
18. Wu Y L, Mooney M A, Cha M S. An experimental examination of foam stability under pressure for EPB TBM tunneling. Tunnelling and Underground Space Technology, 2018, 77: 80−93
19. Hu Q X, Wang S Y, Qu T M, Xu T, Huang S, Wang H B. Effect of hydraulic gradient on the permeability characteristics of foam-conditioned sand for mechanized tunnelling. Tunnelling and Underground Space Technology, 2020, 99: 103377
20. Carigi A, Luciani A, Todaro C, Martinelli D, Peila D. Influence of conditioning on the behaviour of alluvial soils with cobbles. Tunnelling and Underground Space Technology, 2020, 96: 103225
21. Selmi M, Kacem M, Jamei M, Dubujet P. Physical foam stability of loose sandy-clay: A porosity role in the conditioned soil. Water, Air, and Soil Pollution, 2020, 231(5): 251
22. Huang Z Q, Wang C, Dong J Y, Zhou J J, Yang J H, Li Y W. Conditioning experiment on sand and cobble soil for shield tunneling. Tunnelling and Underground Space Technology, 2019, 87: 187−194
23. Xu Q W, Zhang L Y, Zhu H H, Gong Z Y, Liu J G, Zhu Y H. Laboratory tests on conditioning the sandy cobble soil for EPB shield tunnelling and its field application. Tunnelling and Underground Space Technology, 2020, 105: 103512
24. Ling F, Wang S, Hu Q, Huang S, Feng Z. Effect of bentonite slurry on the function of foam for changing the permeability characteristics of sand under high hydraulic gradients. Canadian Geotechnical Journal, 2022, 59(7): 1061−1070
25. Borio L, Peila D. Study of the permeability of foam conditioned soils with laboratory tests. American Journal of Environmental Sciences, 2010, 6(4): 365−370
26. Kim T H, Kim B K, Lee K H, Lee I M. Soil conditioning of weathered granite soil used for EPB shield TBM: A laboratory scale study. KSCE Journal of Civil Engineering, 2019, 23(4): 1829−1838
27. Wang S, Huang S, Zhong J, Zhang S, Hu Q, Qu T, Ye X. Permeability stability calculation model of foam-conditioned soil based on the permeability constant. International Journal for Numerical and Analytical Methods in Geomechanics, 2021, 45(4): 540−559
28. Katagiri J, Kimura S, Noda S. Significance of shape factor on permeability anisotropy of sand: Representative elementary volume study for pore-scale analysis. Acta Geotechnica, 2020, 15(8): 2195−2203
29. Uma K O, Loehnert E P. Hydraulic conductivity of shallow sandy aquifers: Effects of sedimentologic and diagenetic differences. Environmental Geology, 1994, 23(3): 171−181
30. Yu L, Han Z, He J, Li G. Experimental study on the permeability damage mechanism of gravel pack sand control medium in mud hydrate reservoirs. Journal of Coastal Research, 2022, 38(6): 1104−1115
31. Jauregi P, Gilmour S, Varley J. Characterisation of colloidal gas aphrons for subsequent use for protein recovery. Chemical Engineering Journal, 1997, 65(1): 1−11
32. Molaei A, Waters K E. Aphron applications—A review of recent and current research. Advances in Colloid and Interface Science, 2015, 216: 36−54
33. Sun Q, Li Z M, Wang J Q, Li S Y, Li B F, Jiang L, Wang H Y, Lu Q C, Zhang C, Liu W. Aqueous foam stabilized by partially hydrophobic nanoparticles in the presence of surfactant. Colloids and Surfaces A: Physicochemical and Engineering Aspects, 2015, 471: 54−64
34. EFNARC. Specifications and Guidelines for the Use of Specialist Products for Mechanized Tunnelling (TBM) in Soft Ground and Hard Rock. Surrey: EFNARC, 2005
35. Min F L, Song H B, Zhang N. Experimental study on fluid properties of slurry and its influence on slurry infiltration in sand stratum. Applied Clay Science, 2018, 161: 64−69
36. ASTM C143/C143M-20. Standard Test Method for Slump of Hydraulic-Cement Concrete. West Conshohocken: ASTM International, 2020
37. ASTM D2434-22. Standard Test Methods for Measurement of Hydraulic Conductivity of Coarse-Grained Soils. West Conshohocken: ASTM International, 2022
38. Zhao G, Dai C L, Wen D L, Fang J C. Stability mechanism of a

novel three-phase foam by adding dispersed particle gel. Colloids and Surfaces A: Physicochemical and Engineering Aspects, 2016, 497: 214−224

39. Zhong X, Liu D X, Shi X F, Zhao H T, Pei C, Zhu T Y, Shao M L, Zhang F. Characteristics and functional mechanisms of clay-cement stabilized three-phase nitrogen foam for heavy oil reservoir. Journal of Petroleum Science Engineering, 2018, 170: 497−506
40. Wang H, Wang S, Zhong J, Qu T, Liu Z, Xu T, Liu P. Undrained compressibility characteristics and pore pressure calculation model of foam-conditioned sand. Tunnelling and Underground Space Technology, 2021, 118: 104161
41. Zhong J, Wang S, Qu T. Undrained vane shear strength of sand-foam mixtures subjected to different shear rates. Journal of Rock Mechanics and Geotechnical Engineering, 2022, 15(6): 1591−1602
42. Zhang S Q, Pei H F. Determining the bound water content of montmorillonite from molecular simulations. Engineering Geology, 2021, 294: 106353
43. Carn F, Colin A, Pitois O, Vignes-Adler M, Backov R. Foam drainage in the presence of nanoparticle-surfactant mixtures. Langmuir, 2009, 25(14): 7847−7856
44. Jin H J, Zhou W Z, Cao J, Stoyanov S D, Blijdenstein T, de Groot P, Arnaudov L N, Pelan E G. Super stable foams stabilized by colloidal ethyl cellulose particles. Soft Matter, 2012, 8(7): 2194−2205
45. Wang T F, Fan H M, Yang W P, Meng Z. Stabilization mechanism of fly ash three-phase foam and its sealing capacity on fractured reservoirs. Fuel, 2020, 264: 116832
46. Zhao J, Torabi F, Yang J. The synergistic role of silica nanoparticle and anionic surfactant on the static and dynamic CO_2 foam stability for enhanced heavy oil recovery: An experimental study. Fuel, 2021, 287: 119443
47. Binks B P. Particles as surfactants—Similarities and differences. Current Opinion in Colloid & Interface Science, 2002, 7(1−2): 21−41
48. Garbin V, Crocker J C, Stebe K J. Nanoparticles at fluid interfaces: Exploiting capping ligands to control adsorption, stability and dynamics. Journal of Colloid and Interface Science, 2012, 387(1): 1−11
49. Tzoumaki M V, Karefyllakis D, Moschakis T, Biliaderis C G, Scholten E. Aqueous foams stabilized by chitin nanocrystals. Soft Matter, 2015, 11(31): 6245−6253
50. Yekeen N, Manan M A, Idris A K, Padmanabhan E, Junin R, Samin A M, Gbadamosi A O, Oguamah I. A comprehensive review of experimental studies of nanoparticles-stabilized foam for enhanced oil recovery. Journal of Petroleum Science Engineering, 2018, 164: 43−74
51. Zhu W X, Zheng X H, Li G M. Micro-bubbles size, rheological and filtration characteristics of Colloidal Gas Aphron (CGA) drilling fluids for high temperature well: Role of attapulgite. Journal of Petroleum Science Engineering, 2020, 186: 106683